THE JOURNAL OF PHYSICAL CHEMISTRY A

Article

pubs.acs.org/JPCA

Ion-Induced Reorientation and Distribution of Pentanone in the Air–Water Boundary Layer

Kathryn L. Plath, Nicholas A. Valley, and Geraldine L. Richmond*

Department of Chemistry, University of Oregon, Eugene, Oregon 97403, United States

ABSTRACT: Organic material at the surface of atmospheric aerosols is ubiquitous and plays an important role in Earth's atmosphere. Small ketones, such as 3-pentanone, are found in aerosols and as surface-active species on aerosols. This study uses 3-pentanone as a model ketone to understand how such molecules adsorb at the vapor–water interface on aqueous solutions containing sulfate, carbonate, or chloride ions. By combining surface spectroscopic experiments with computational methods, very detailed information about the molecular bonding, geometries, and surface orientation of 3-pentanone as a function of depth has been obtained. The results show that, for pure water, 3-pentanone resides at the topmost surface of water with the carbonyl pointing into the aqueous phase where it is weakly solvated. For Na_2SO_4-containing solutions, we found that sulfate ions in the boundary layer provoke changes in the geometry and interfacial position of 3-pentanone that are not seen in solutions containing sodium chloride or sodium carbonate. The results provide important insight into the behavior of ketones in the presence of salts at the surface of aerosols in the atmosphere.

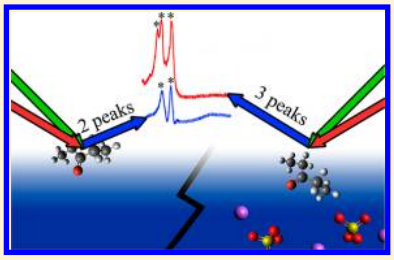

1. INTRODUCTION

Organic compounds comprise a significant fraction of tropospheric aerosols, and their presence affects the climate-forcing ability of these aerosols.[1] However, the extent of the aerosols' ability to force climate is very uncertain.[2] It has been suggested that this uncertainty results from the absence of molecular-level information with respect to aerosol composition, structure, and chemistry,[3,4] prompting interest in the effects of organic matter on aerosol surfaces, aerosol bulk properties, and the mass accommodation of organic matter in aerosols.[5] Aldehydes and ketones are a particularly interesting class of compounds with a complicated and inadequately understood role in the environment.[6,7]

Ketones enter the atmosphere both from direct emissions and from the oxidation of volatile organic compounds (VOCs) as a part of secondary organic aerosols (SOAs). They undergo a wide variety of chemical reactions with other atmospheric constituents: They can be oxidized to form carboxylic acids; they react with ammonium sulfate, sulfuric acid, amines, and other NO_x compounds; they are known to react with OH and other radicals; and they undergo oligomerization and aldol condensation in the aqueous phase. Although considered to be a volatile species, small aldehydes and ketones have been measured in cloudwater and rainwater.[8−13] The lack of agreement between field measurements and computer simulations based on volatility suggest that small aldehydes and ketones partition to the aerosol phase to a greater degree than models suggest.[6,7] This study examines the nature of this surface partitioning in response to specific ion effects using a combination of vibrational sum frequency spectroscopy and computational methods. Previous vibrational sum frequency (VSF) spectroscopy studies of aldehydes and ketones at the air–water interface have been limited to the small, atmospherically abundant molecules formaldehyde, acetaldehyde, and acetone.[14−17] The more complex 3-pentanone is presented here as a representative compound of longer-chain ketones, which strike a different balance between hydrophilic and hydrophobic properties, for study at the air–water interface.

Inorganic salts in atmospheric aerosols affect bulk properties, such as growth and reactivity.[5] The air–water interface of aerosols is influenced by the presence of inorganic salts, which are ubiquitous in these aerosols. Studies of the air–water interface have explored the impact of ions in solution on the behavior of organic compounds, such as carboxylic acids.[18−21] The ions explored in this study (NaCl, Na_2SO_4, and Na_2CO_3) are of particular interest because of their high concentrations in atmospheric waters.[5,22−25]

Along with its importance to atmospheric aerosols, ion behavior at the air–water interface is of general scientific interest. The role of ions at the air–water interface has been the subject of many studies and much discussion. In recent years, experiments have demonstrated that ions are likely present in the interfacial layer.[26−30] Using VSF spectroscopy, many studies have been undertaken to elucidate the behavior of ions at the air–water interface. The effect on the water structure of anions has been widely studied using VSF spectroscopy, and the sulfate ion's vibrational stretching modes recently have been probed as well.[21,24,31−39] Recent advances in phase-sensitive sum frequency spectroscopy have further elucidated the behavior of ions at the air–water interface and described the magnitude and direction of the electric field produced by the ions near the surface.[40,41] Hua et al. noted that the direction of the electric field is opposite for sulfate and carbonate solutions compared to chloride solutions. They further asserted that

Received: August 15, 2013
Revised: October 9, 2013
Published: October 31, 2013

ACS Publications © 2013 American Chemical Society

Na_2SO_4 produces a stronger electric field than Na_2CO_3 or NaCl.[40]

VSF spectroscopy probes surface-specific vibrational modes and can be tuned to study the particular vibrational modes of species in the interfacial layer. VSF is a powerful technique because it reflects both composition and molecular orientation in the interfacial region. Theoretical calculation of VSF spectra provides further insight into the specific source of VSF spectral features and can directly connect experimental measurements and results of molecular dynamics calculations. VSF spectra can be calculated in a variety of ways.[17,42−47] Here, a combination of separate classical molecular dynamics and gas-phase density functional theory calculations were used to compose theoretical spectra of 3-pentanone. A similar approach has achieved reasonable results in various works for water[17,48−52] and succinic acid.[53]

In this study, VSF experiments were utilized to detect changes in the CH, C═O, and OH vibrational stretching responses from 3-pentanone and water as they were affected by the presence of inorganic ions. The ions chosen for this study (NaCl, Na_2SO_4, and Na_2CO_3) all contain the sodium cation, which is not expected to strongly affect the interfacial structure, in order to focus on the varying impact of the anion. Theoretical calculations of the dynamics and VSF spectra of 3-pentanone were used to reveal further molecular-level details. The VSF spectroscopic data were analyzed together with computational results to provide a complete molecular-level picture of 3-pentanone at the air−water interface in the presence of inorganic salts.

2. BACKGROUND

Vibrational sum frequency (VSF) spectroscopy is a surface-specific technique that provides insight into the aqueous interface. The VSF signal results from the spatial and temporal overlap of, in this work, a fixed-energy 800-nm beam and a tunable IR beam at a noncentrosymmetric interface. The signal is further dependent on the number density, orientation, and IR and Raman transition strengths of vibrational modes resonant with the IR frequency. This signal can describe the intermolecular interactions, bond strengths, and orientations of molecules at the interface. Several excellent references on the technique are available.[54−73]

The intensity of the generated sum-frequency signal is proportional to the squared second-order susceptibility, $\chi^{(2)}$, and the intensities of the incoming visible and IR beams. The second-order susceptibility has contributions from both resonant and nonresonant components. The individual resonant components of the second-order susceptibility are proportional to the number of contributing molecules, N, and the orientationally averaged molecular hyperpolarizability, $\langle\beta_i\rangle$

$$\chi^{(2)}_{\mathrm{R},i} = \frac{N}{\varepsilon_0}\langle\beta_i\rangle \tag{1}$$

VSF spectra are fit to deconvolve the nonresonant signal and the individual resonant vibrational modes. The method follows a fitting routine proposed by Bain and accounts for the homogeneous and inhomogeneous line widths of the individual vibrational modes.[74]

$$\chi^{(2)} = \chi^{(2)}_{\mathrm{NR}} e^{i\psi} + \sum_{\nu}\int_{-\infty}^{\infty} \frac{A_\nu e^{i\phi_\nu} e^{-[(\omega_\mathrm{L}-\omega_\nu)/\Gamma_\nu]^2}}{\omega_\mathrm{L} - \omega_\mathrm{IR} + i\Gamma_\mathrm{L}}\, d\omega_\mathrm{L} \tag{2}$$

The first term in eq 2, $\chi^{(2)}_{\mathrm{NR}}$, is the nonresonant second-order susceptibility, and the second term is the sum of the individual resonant second-order susceptibilities. The resonant second-order susceptibility is fit as a convolution of the homogeneous line widths of the individual vibrational modes, Γ_L, and the inhomogeneous broadening, Γ_ν. The A_ν term describes the transition strength and is proportional to the product of the number of contributing molecules and the orientationally averaged IR and Raman transition probabilities. The frequencies of the Lorentzian, IR, and resonant vibrational mode are given by ω_L, ω_IR, and ω_ν, respectively, and ϕ_ν is the phase of each resonant mode. Changes in the sum frequency signal and the resultant spectral fits can be attributed to changes in the number of contributing molecules, the orientation of the molecules, and changes in the bond energies of the resonant modes.

The specification of incoming and outgoing polarization schemes in sum frequency generation can be used to extract information on the orientation of the resonant modes contributing to the signal. Of the 27 elements of $\chi_{(2)}$, only four are both nonzero and unique. Using specific known polarizations of the incoming visible and IR beams and the outgoing sum frequency light, it is possible to probe these unique elements. The polarization schemes are described in the order sum frequency beam, visible beam, and IR beam, with S-polarized light perpendicular to the plane of incidence and P-polarized light parallel to the plane of incidence. Thus, in these experiments, the SSP scheme is used to probe dipole transition moment components perpendicular to the plane of the interface.

3. EXPERIMENTAL DETAILS

3.1. Laser Systems. The VSF spectra were collected on two separate laser systems. The first system is a broad bandwidth sum frequency system and was used to collect spectra in the mid-IR region between 1600 and 1900 cm^{-1}. This is a newly built system based on a design similar to that of systems that have been previously described.[21,75,76] Briefly, a Libra Ultrafast laser system (Coherent) produces spectral output centered at ∼800 nm with a pulse length of ∼100 fs and an average power of 3 W. The output beam is split, with ∼1.5 W used for the visible line and ∼1.5 W going to an optical parametric amplifier (OPerA Solo, Light Conversion) for the IR line. The visible beam is sent through a 4f optical slicer to produce pulses in the picosecond range. Both the IR and visible beams are propagated to the air−water interface in a copropagating geometry. The IR and visible beams are angled to the interface at 45° and 60°, respectively, and overlapped in time and space to generate sum frequency pulses. The resulting sum frequency signal is collected, filtered to remove stray 800-nm light, dispersed with a holographic 1800 groove/mm spectrograph (Shamrock 303iB, Andor), and detected with a thermoelectrically cooled charge-coupled device (CCD, Newton 920, Andor). To minimize IR light loss by absorption of water vapor in the ambient air, the IR line, the air−water interface, and the sum frequency signal were all contained within a purged air volume. The purged air was generated using a Pneudri MiDAS air dryer (Parker Domnick Hunter).

A second experimental setup was used to collect data over the region from 2700 to 4000 cm^{-1} and has been described elsewhere.[77−79] Briefly, the sum frequency signal is generated using 800-nm light from a Spectra Physics Spitfire Pro XP lased and tunable IR light produced from a home-built optical

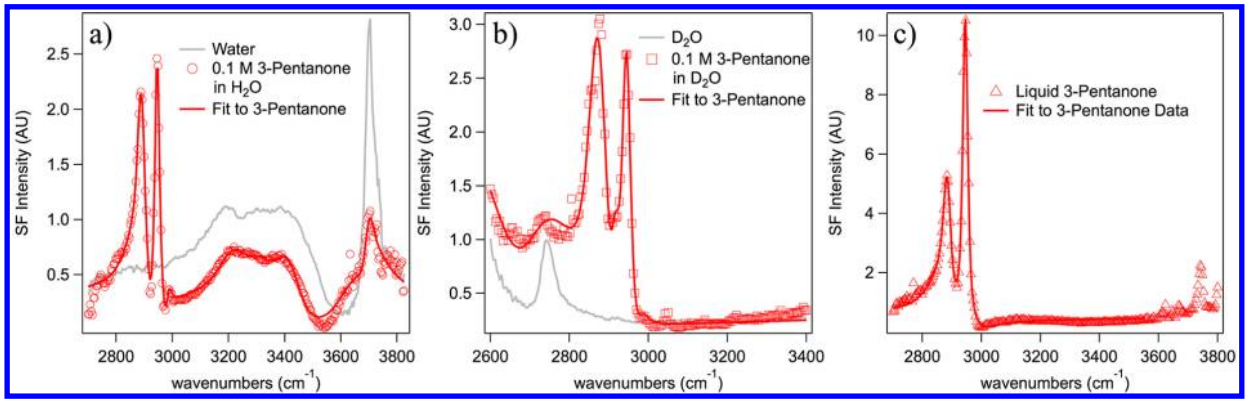

Figure 1. VSF spectra of 3-pentanone (a) in H_2O, (b) in D_2O, and (c) as neat liquid. The data are represented by symbols, whereas the solid lines are the spectral fits. Spectra were obtained in the SSP polarization scheme. In panel a, the gray trace is the VSF spectrum of neat water for comparison. In panel b, the gray trace is the VSF spectrum of neat D_2O.

parametric amplifier. The IR and visible beams copropagate to the air−water interface at 67° and 56°, respectively, from the surface normal. The resultant sum frequency signal is measured using a thermoelectrically cooled CCD (Princeton Instruments). The spectra were collected at 3 cm^{-1} increments over the tunable range. All of the spectra, from both experiments, were normalized to the nonresonant sum frequency response of a bare gold surface. The spectra presented in this work were all collected using the SSP polarization scheme. SPS polarization for similar ketones resulted in insufficient signal, and so, was not investigated for 3-pentanone. Spectra of all 3-pentanone solutions used concentrations of 0.1 M 3-pentanone, as lower concentrations resulted in inconsistent signal and higher concentrations resulted in excessive scattering of the 800-nm light. Wavelengths were calibrated based on a polystyrene standard. All measurements were made at ambient temperature, ~20 °C. Experimental peak positions are reported with uncertainties in the fit. Peak positions are also subject to error from the resolution of the instrumentation, which is on the order of 12−15 cm^{-1}. The total error in reported peak positions is therefore expected to be on the order of 20 cm^{-1}.

3.2. Sample Preparation. 3-Pentanone (Reagent Plus, ≥99.5%), NaCl (Reagent Plus, >99.5%), Na_2SO_4 (BioXtra, ≥99.0%), and Na_2CO_3 (ACS reagent, anhydrous) were purchased from Sigma-Aldrich. 3-Pentanone-2,2,4,4-d_4 was purchased from C/D/N Isotopes. All solutions were prepared fresh with >18 MΩ·cm water. The NaCl and Na_2CO_3 salts were baked in an oven at 220 °C for at least 72 h before use to eliminate contaminants. All other chemicals were used as received. All glassware was cleaned using concentrated H_2SO_4 and NOCHROMIX and thoroughly rinsed with >18 MΩ·cm water.

3.3. Classical Molecular Dynamics Methods. Classical molecular dynamics (MD) calculations were performed using the Amber 12 suite of programs.[80] Starting configurations were created using PACKMOL.[81] Starting configurations consisted of 900 water molecules and 2 or 16 3-pentanone molecules in a cube with sides of 30 Å, corresponding to an overall concentration of approximately 0.12 or 1 M, respectively. The higher concentration provided a bulk concentration more in line with the experimental bulk concentration, but resulted in negligible differences in the conformational populations, orientations, and calculated spectra. Simulations with sodium sulfate were performed by adding 8 sodium ions and 4 sulfate ions to make a salt concentration of 0.25 M. A water slab with two surfaces was created by expansion of one of the box dimensions to 120 Å and application of periodic boundary conditions.

Energy minimization of the initial system was performed using a combination of steepest-descent and conjugate-gradient methods. Minimized structures were equilibrated by evolution through 2 ns of MD simulation. Each system was further evolved for 50 ns, with atomic coordinates recorded every 100 fs for a total of 500000 data points. The simulations were performed using a time step of 1 fs. Fully polarizable models were used. Water was simulated using the POL3 model,[82] the model for 3-pentanone was constructed using a fully atomistic model based on the Amber FF02EP force field,[83] and the model for the ions was that developed by Jungwirth et al.[84] The system temperature was set at 298 K, and Langevin dynamics was used to propagate dynamics with a leapfrog integrator. The particle mesh Ewald technique was used for calculating long-range electrostatic interactions, with a force cutoff set to 12 Å. Water molecules were held rigid by means of the SHAKE algorithm to increase computational throughput and speed of data collection.

Distances from the water surface were calculated using the Gibbs dividing surface determined from a hyperbolic tangent fit to the water density profile. To correct for possible drift of the water surface over the length of the simulation, the coordinates of each data point were shifted so that the center of mass of the water system remained constant. Data were collected using both water−vacuum interfaces, and angles relative to the surface were measured from the surface normal pointing into the vacuum phase.

3.4. Quantum Mechanical Methods. The calculations presented in this work were performed using the NWChem program package.[85] Full geometry optimization and harmonic vibrational frequency calculations for isolated 3-pentanone molecules were performed using the B3LYP exchange-correlation functional and a 6-311++G(2d,2p) basis set. Polarizabilities and dipole moments at displaced geometries were calculated using the same level of theory.

Vibrational sum frequency intensities were calculated by inspecting the second-order linear susceptibility tensor. The tensor was constructed using polarizability and dipole moment derivatives with respect to the vibrational normal coordinates combined according to the expression

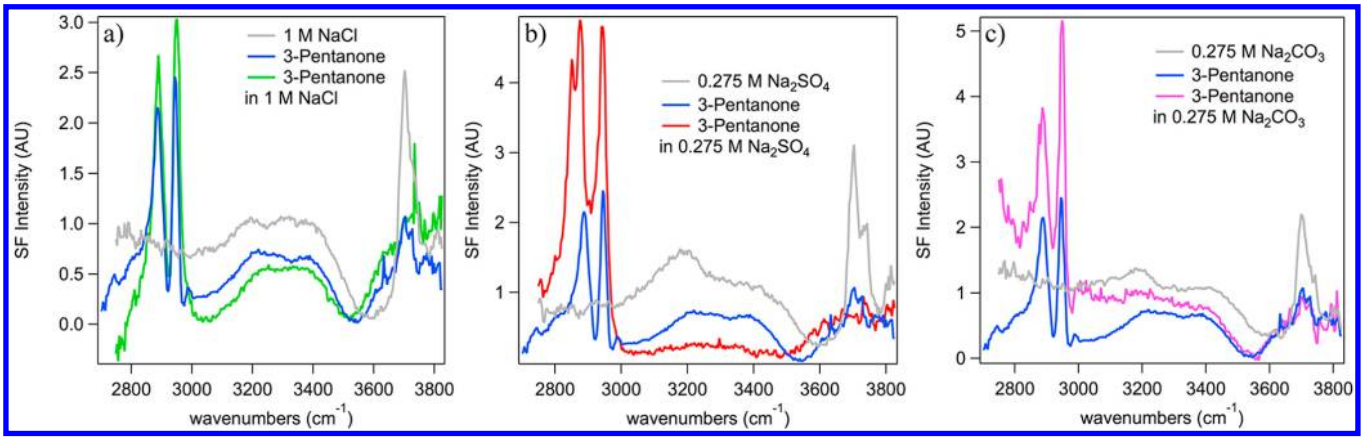

Figure 2. VSF spectra of 3-pentanone in (a) 1 M NaCl solution, (b) 0.275 M Na_2SO_4 solution, and (c) 0.275 M Na_2CO_3 solution. In each panel, the gray trace is the neat-water spectrum; the blue trace is the VSF spectrum of 0.1 M 3-pentanone in water, for reference. All data were recorded in the SSP polarization scheme.

$$\chi^{(2)}_{ijk} \propto \sum_{a,b,c} C_{abc} \frac{\partial \alpha_{ab}}{\partial Q_q} \frac{\partial \mu_c}{\partial Q_q} \tag{3}$$

where α is the molecular polarizability, μ is the dipole moment, ∂Q_q is the displacement of normal mode q, and C is a geometrical factor relating the molecular and laboratory reference frames. Derivatives were calculated using three-point finite differentiation.

4. RESULTS AND DISCUSSION

4.1. Water and CH Vibrational Stretching Modes. The spectrum of 3-pentanone in D_2O is shown in Figure 1b. The gray trace in Figure 1b is the neat-D_2O VSF spectrum for comparison. The energy of O−D vibrational modes is red-shifted from the O−H analogues in Figure 1a. There are two modes associated with OD vibrational stretching modes: the "free-OD" vibrational stretching modes at 2715 cm^{-1} and the more coordinated OD vibrational stretching mode at 2578 cm^{-1}.[86] Figure 1b shows the spectrum fit with four peaks that are assigned as CH vibrational stretching modes. These peaks are centered at 2884 ± 1, 2913 ± 1, 2944 ± 1, and 2979 ± 4 cm^{-1}. Note that the instrument resolution is ∼12−15 cm^{-1}, which will contribute additional uncertainty to all reported peak locations. These CH vibrational modes are the same as those seen in the VSF spectrum of neat 3-pentanone (Figure 1c).

To rule out the presence of the other forms of ketones known to exist in equilibrium in water solutions, which are the enol and geminal diol, the spectra of 3-pentanone in D_2O and as a neat liquid were compared. In the VSF spectrum, the alcohol vibrational stretching mode of either the enol or diol would appear between 2800 and 3100 cm^{-1} and is expected to be low in intensity and broad.[87] In the solution with D_2O, the OD vibrational mode is red-shifted to <2500 cm^{-1} and is not observable in this experiment. Thereby, the presence of the enol or diol species would be evident in the 3-pentanone spectrum in H_2O and D_2O through differences in this region. The observed lack of changes provides confidence that non-negligible quantities of the enol or diol species are not present.

The presence of 3-pentanone clearly causes a change in the H_2O spectrum, as seen in Figure 1a. Several prominent peaks associated with CH vibrational stretching modes are located between 2700 and 3000 cm^{-1}. Spectral fitting identified four separate modes that were necessary to reproduce the experimental line shape. These peaks occur at 2896 ± 1, 2910 ± 2, 2942 ± 1, and 2982 ± 3 cm^{-1}. Assignments of the vibrational modes will be discussed later. One peak at 3632 cm^{-1}, which can be assigned to the topmost water molecules interacting with the organic species, is also observed in the spectrum of 3-pentanone in H_2O.[88] The continuing presence of the "free-OH" vibrational mode suggests that, at this concentration of 3-pentanone, there is incomplete surface coverage.

As a part of this study, we monitored the general changes in the water spectrum in the presence of 3-pentanone and salt species. A more thorough description of the fitting of the neat-water spectrum can be found in the literature.[49,52,86,89−93] The free-OH vibrational mode resides at ∼3700 cm^{-1} and is assigned to uncoupled OH oscillators pointing away from the bulk water. Three peaks are found in the neat-water VSF spectrum between 3200 and 3500 cm^{-1} that arise from the various OH vibrational stretching modes associated with water molecules in a hydrogen-bonded network. The mode at ∼3460 cm^{-1} gives rise to broad spectral intensity and corresponds to OH groups near the surface and pointing toward the bulk. Two modes associated with more coordinated water molecules that reside deeper in the interface are at ∼3200 and ∼3300 cm^{-1}. All spectra also include a nonresonant background signal.

Addition of inorganic salts to the neat-water spectrum has been discussed previously.[24,28,39,84,94,95] In these studies, the cation remained constant to focus on the impact of the anion on the orientation and distribution of 3-pentanone at the air−water interface. Previous work on NaCl solutions has shown that the water structure is not significantly altered by the ions and that no additional peaks appear.[39] In Na_2SO_4 and Na_2CO_3 solutions, the impact of the ions on the water structure is more pronounced, and an additional peak at ∼3150 cm^{-1} is added, as discussed elsewhere.[24] In Figure 2, each panel has a gray trace of the spectrum of the corresponding salt solution and a blue trace of 3-pentanone in water for comparison. The VSF spectrum with 3-pentanone in the presence of 1 M NaCl is similar to the spectrum without ions present, as is seen in Figure 2a. However, there is an increase in the intensity of the peaks between 2800 and 3000 cm^{-1}. We suggest that the small intensity increase is due to the weak salting-out of 3-pentanone by NaCl. The peak positions of the four CH vibrational modes of 3-pentanone are relatively unchanged compared to those of the solutions without salt. Spectral fitting places these four CH vibrational modes at 2885 ± 3, 2895 ± 1, 2946 ± 1, and 2980

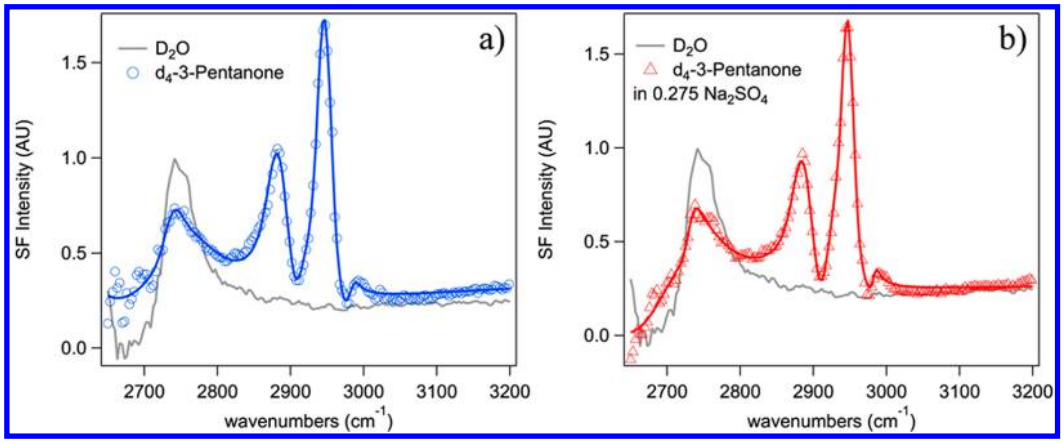

Figure 3. VSF spectra of 0.1 M 3-pentanone-d_4 in (a) D_2O and (b) 0.275 M Na_2SO_4 solution in D_2O. The data are represented by symbols, and the solid lines are the results of spectral fitting. In each panel, the gray trace is the neat-D_2O spectrum for comparison.

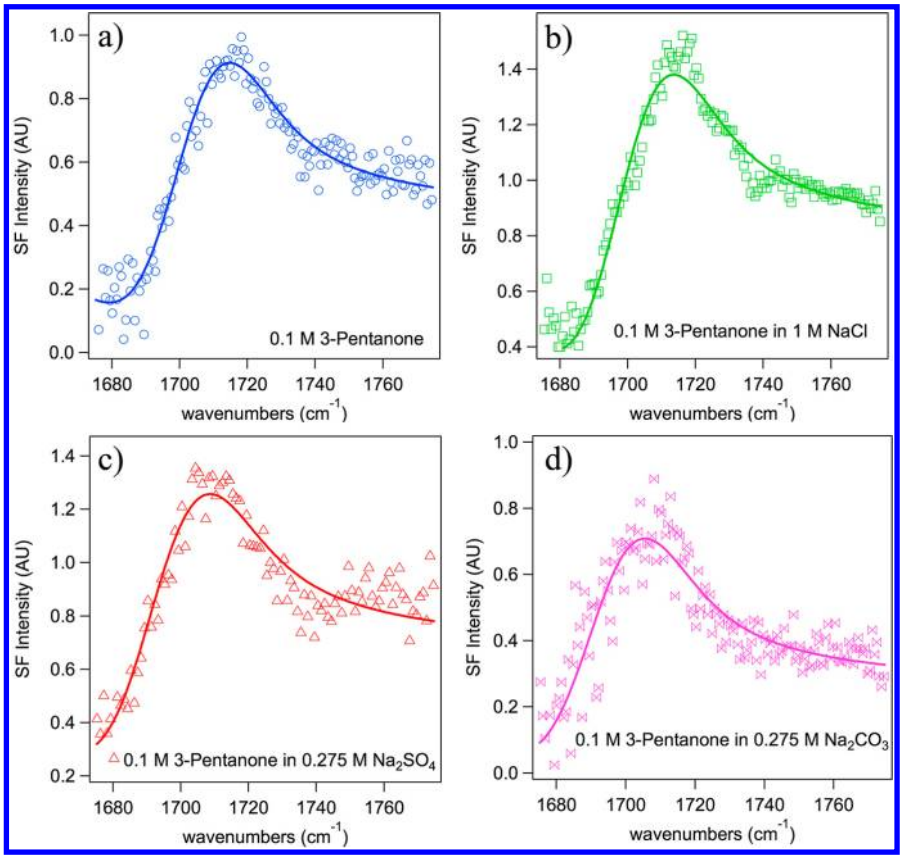

Figure 4. VSF spectra of the carbonyl vibrational stretching mode of 0.1 M 3-pentanone in (a) H_2O, (b) 1 M NaCl solution, (c) 0.275 M Na_2SO_4 solution, and (d) 0.275 M Na_2CO_3 solution. The data are presented as symbols, and the solid lines represent the spectral fits. All data were recorded in the SSP polarization scheme.

$\pm$ 5 cm^{-1}. Based on the lack of significant change upon the addition of NaCl to the solution, we conclude that the behavior of 3-pentanone in the interfacial region is not substantially altered by the presence of the salt.

In contrast, Na_2SO_4 in solution has a marked effect on 3-pentanone at the surface, as shown in Figure 2b. These changes occur in both the intensity and the line shape in the region of the CH vibrational stretching modes. The peaks in the CH stretching mode region, between 2800 and 3000 cm^{-1}, are more intense than those in the spectrum of 3-pentanone in NaCl solutions. Sodium sulfate has a stronger salting-out potential than sodium chloride,[96] which might be partially responsible for the increase in intensity of the CH mode signal. Also, there is an additional peak at lower energy. To reproduce the line shape of 3-pentanone in Na_2SO_4 solutions, an additional peak was added at 2858 $\pm$ 1 cm^{-1}, whereas the four peaks at 2879 $\pm$ 1, 2910 $\pm$ 2, 2948 $\pm$1, and 2970 $\pm$ 20 cm^{-1} are similar to the CH vibrational modes of 3-pentanone in H_2O. This new peak at ~2860 cm^{-1} is not explained by the salting-out phenomenon. The origins of this peak will be discussed later.

The coordinated OH vibrational modes that are present in the spectrum of Na_2SO_4 solutions and in the spectrum of 3-pentanone in H_2O are less intense in the spectrum of 3-

dx.doi.org/10.1021/jp408188x | J. Phys. Chem. A 2013, 117, 11514−11527

pentanone in Na_2SO_4 solutions. As with previous studies of Na_2SO_4 solution and the Na_2SO_4−3-pentanone solution, an additional mode is observed at 3190 cm^{-1}. We attribute this mode to OH vibrational modes of water interacting with ions in solution.[24]

The effect of sodium carbonate solutions on 3-pentanone behavior at the air−water interface was also probed. Sodium carbonate is known to cause a stronger salting-out effect than either sodium chloride or sodium sulfate. We expect this to cause a more intense signal of 3-pentanone modes in the VSF spectrum. As can be seen in Figure 2c, the spectrum of 3-pentanone in 0.275 M Na_2CO_3 solution shows increased intensity in the CH vibrational modes compared to the spectrum of 3-pentanone in H_2O or 3-pentanone in NaCl or Na_2SO_4 solutions. Although there is an increase in the intensity, the spectral fits of the CH vibrational modes do not display significant shifts in the peak positions. The peaks of 3-pentanone in sodium carbonate solutions are observed at 2890 ± 10, 2897 ± 2, 2945 ± 1, and 2985 ± 4 cm^{-1}.

The coordinated water vibrational modes in the spectrum of 3-pentanone in Na_2CO_3 solution are less intense compared to those in Na_2CO_3 solution or aqueous 3-pentanone solution. As in the sulfate solutions, an additional mode for water molecules interacting with ions in solution at ∼3200 cm^{-1} is apparent. The intensity changes observed in the spectra of 3-pentanone in NaCl and Na_2CO_3 solutions do not show inconsistencies with predicted "salting-out" behavior; however, the spectral changes of 3-pentanone in Na_2SO_4 solutions are indicative of behavior that cannot be explained without additional effects.

The origins of the new CH vibrational mode, at ∼2860 cm^{-1}, in the 3-pentanone in Na_2SO_4 solution were investigated further. To accomplish this, the spectrum of 3-pentanone-d_4 [$CH_3CD_2C(=O)CD_2CH_3$] was collected. The spectrum in Figure 3a is that of 0.1 M 3-pentanone-d_4 in D_2O, and the gray trace is that of neat D_2O for comparison. The 3-pentanone-d_4 spectrum is fit with three CH vibrational modes, the peak positions of which are 2891 ± 2, 2941 ± 1, and 2982 ± 4 cm^{-1}. All of the CH peaks must be due to methyl vibrational stretching modes, as the CD_2 vibrational stretching modes are shifted to ∼2200 cm^{-1}.

The spectrum of 3-pentanone-d_4 in 0.275 M Na_2SO_4 in D_2O is shown in Figure 3b. The VSF spectrum of 3-pentanone-d_4 does not change appreciably in the Na_2SO_4 solution as compared to the aqueous solution. By comparing the spectrum of 3-pentanone-d_4 in Na_2SO_4 solution (Figure 3b) to that of 3-pentanone in Na_2SO_4 solution (Figure 2a), we conclude that the intensity of the additional peak at 2857 cm^{-1} for 3-pentanone in Na_2SO_4 solution requires the presence of the methylene moieties.

4.2. C═O Vibrational Stretching Mode. The orientation of the carbonyl moiety of 3-pentanone at the air−water interface can also be probed to elucidate the effect of the sulfate ions on the 3-pentanone molecules. The spectra of 3-pentanone in H_2O, 1 M NaCl, 0.275 M Na_2SO_4, and 0.275 M Na_2CO_3 solutions are presented in Figure 4. Each of these spectra shows a single peak. Additional peaks did not improve the fits. Furthermore, there are no significant changes in the peak position, intensity, or line width in the presence of any of the inorganic salts. The 3-pentanone carbonyl stretching mode lies at 1700 ± 11 cm^{-1} in H_2O, at 1698 ± 1 cm^{-1} in NaCl, at 1696 ± 4 cm^{-1} in Na_2SO_4, and at 1701 ± 1 cm^{-1} in Na_2CO_3. All of these values are within the resolution of the experiment. The Gaussian line widths from the spectral fitting are all in the range of 15−30 cm^{-1}. The lack of change in the spectra of the carbonyl vibrational stretching mode of 3-pentanone in the presence of various ions in solution, in contrast to the CH stretching region, shows no evidence of changes in population, bonding environment, and orientation at the interface, regardless of the identity of the ions.

Sodium sulfate provokes unique changes in the 3-pentanone spectrum that are not seen in solutions of sodium chloride or sodium carbonate. Of the four CH vibrational modes observed in the 3-pentanone spectrum, three modes are attributed to methyl vibrational stretches, and one mode appears to be due to methylene vibrational stretching. Furthermore, the CH stretching peak that appears in Na_2SO_4 solution is due to a methylene vibrational stretching mode. We used theoretical methods to more fully explore the underlying cause for these changes in the VSF spectra. Given the spectral changes of 3-pentanone in sodium sulfate solutions, we focused on understanding this behavior, whereas the spectral intensity changes of 3-pentanone in sodium chloride and sodium carbonate salts might simply be indicative of salting-out behavior.

4.3. Calculated Structures and Spectra of 3-Pentanone. To further understand the experimental results, computational modeling of 3-pentanone was performed using DFT and classical MD. MD analysis of 3-pentanone at the air−water interface provides insight into the conformers present and the orientation of the molecules relative to the surface. Because of the volatility of 3-pentanone, experimental surface tension measurements were unreliable, and a surface concentration could not be determined. Although negligible change was observed in the calculated properties reported here for the two surface concentrations simulated, it cannot be confirmed that the simulated surface concentrations are representative of the exact experimental conditions. Complementing this, DFT provides mode assignments and spectral intensities for the various observed peaks in the VSF spectra. Results of the molecular dynamics calculations of 3-pentanone in water show that the organic molecules mainly reside in the topmost portion of the interfacial layer. The molecules orient with the oxygen of the carbonyl pointing slightly into the bulk (distribution centered around 20−30° into the bulk). This orientation keeps the hydrophobic hydrocarbons in the vapor phase and away from bulk water.

Gas-phase DFT calculations of 3-pentanone revealed that there are several unique types of conformers. The main conformers of 3-pentanone arise from minima present in the OCCC dihedral angles, one at 0° (the A formation) and one or two between 60° and 110° (the G formation). The 3-pentanone molecule has two organic chains that can each adopt either the A or G formation relative to the carbonyl bond. The two chains, which can independently be in either of the two formations, leads to a total of four unique combinations of A and G formations presented in Figure 5. Each conformer is named by a two letter designation for the formation each chain adopts and, in the case of GG conformers, an additional a or s to signify that the two chains are antarafacial (opposite faces of the molecule) or suprafacial (same side of the molecule). In the gas-phase DFT calculations, based on a Boltzman distribution and considering degeneracy, the dominant structure (50.4%) is the conformer with both OCCC dihedral angles in the A formation (AA). This is followed by the AG conformation comprising the majority of the remaining gas-phase structures at 41.5%.

dx.doi.org/10.1021/jp408188x | J. Phys. Chem. A 2013, 117, 11514−11527

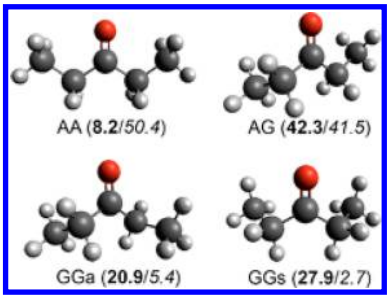

Figure 5. Representations of the conformers of 3-pentanone found by DFT calculations. The bold number below each structure is the percentage of structures with this conformation in the MD simulations of 3-pentanone in water. The number in italics is the percentage of structures with this conformation based on a Boltzmann distribution using DFT energies, approximating gas-phase contributions.

Structures of the 3-pentanone molecules in the MD calculations were then matched with the DFT conformers by interrogation of the OCCC dihedral angles. To determine the effects of solvation, MD calculations were performed on a periodic water box. In water, the AG conformer was found to be most common (49.8%), followed by the AA conformation (27.0%). Structures with both dihedrals in the G formation, GGa (13.4%) and GGs (9.5%), also became more favorable. As opposed to the gas-phase results, the vast majority of structures had at least one dihedral in the G formation. In the MD trajectories, which modeled 3-pentanone at the air−water interface, the conformational distribution continued to show changes compared to the gas-phase DFT results and bulk MD calculations. At the air−water interface, the AG conformer remained most common (42.3%), and structures in which both dihedrals were in the G formation, GGs (27.9%) and GGa (20.9%), became much more favorable at the expense of the AA conformation (8.2%). This change in the conformational contributions is attributed to the greater ability of the G formation to concurrently allow solvation of the carbonyl oxygen while keeping the hydrophobic tails from disrupting the water structure. In the geometry of the A formation, the carbonyl and hydrophobic groups point in roughly the same direction, preventing the molecule from adopting as favorable arrangements as the G formation.

Using orientational and conformational information from the MD calculations and VSF intensities calculated using DFT, theoretical spectra were computed. The complex nature of VSF spectroscopy combined with the specific computational approach used, in certain cases, can lead to unreliable peak intensities and positions. Assignments made using calculated spectra are tentative, but consistent with experimental spectral data presented here, as well as assignments made for similar molecules elsewhere.[87,97] Surface spectra were calculated for both 3-pentanone and 3-pentanone-d_4. The CH vibrational stretching region is shown for both plain (Figure 6a) and partially deuterated (Figure 6b) forms. In both cases, there are two major groupings of peaks. Beneath the composite spectra, the spectral contributions of the various conformers of 3-pentanone are shown and provide a more detailed view of the sources of the peaks in the experimental spectrum. Care has been taken to properly account for enantiomers of chiral structures.

In 3-pentanone, one of the major groupings is centered at ∼2890 cm^{-1} and includes modes with both methyl and methylene symmetric stretch contributions from various conformers. The second grouping, ∼2955 cm^{-1}, is due to methyl asymmetric stretching modes. Overall, there is strong agreement with experiment (Figure 1) in the number and spacing of peaks observed. In comparison with the experimental spectrum, the relative intensity of the 2890 cm^{-1} peak is overestimated in the theoretical spectrum. This might be due to a number of factors; however, a likely cause is the representation of the orientational and conformational distributions by a finite set of static structures and orientations.

The agreement between the theoretical and experimental spectra of 3-pentanone allows mode assignments to be made for the experimental spectral fits and verifies the accuracy of classical MD for further analysis and calculations including sodium sulfate. The experimental peak at 2896 cm^{-1} mainly corresponds with the methylene symmetric vibrational stretching mode of the GGs conformer in the theoretical results. At 2910 cm^{-1}, the major contributor is the methyl symmetric vibrational stretching mode of the AG conformer. The experimentally observed prominent peak at 2942 cm^{-1} has contributions from several conformers, according to the calculation results; however, the largest contribution is the methyl asymmetric vibrational stretching mode of the AG conformer. The experimentally observed weak peak at 2982 cm^{-1} is not predicted by the theoretical spectrum. This peak is

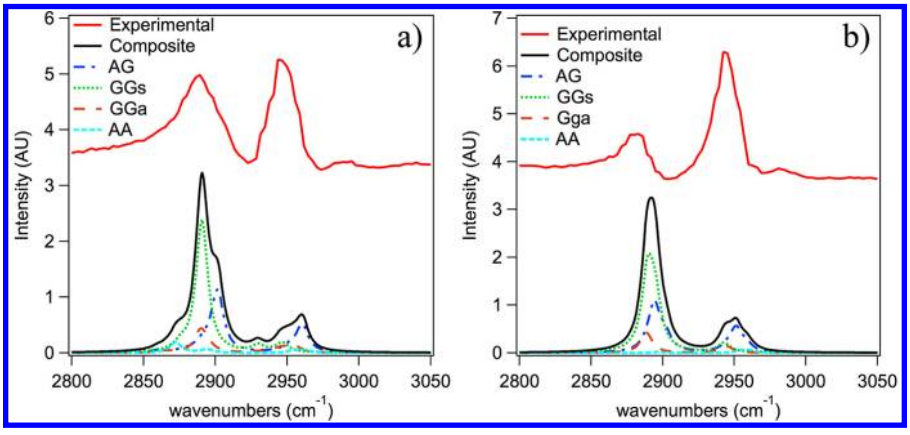

Figure 6. Comparison of the modeled spectrum (lower black trace) with the observed VSF spectrum (red top trace) for (a) 3-pentanone and (b) 3-pentanone-d_4. The black solid trace represents the composite spectrum of all observed conformers and their relative populations. The spectra resulting from the individual conformers are presented underneath the black trace.

tentatively assigned to a Fermi resonance involving symmetric methyl vibrational stretching modes and overtones of the methyl bending modes, as has been assigned in several other sum frequency spectra of small organic molecules.[87,97] The level of theory employed here does not include the interactions necessary to predict the existence of Fermi resonances.

The theoretical spectrum of 3-pentanone-d_4, presented in Figure 6b, also shows strong agreement with the experimental spectrum. The theoretical spectrum can again be described as two major peaks, and each of these peaks has contributions from several conformers of the molecule. The theoretical work accurately re-creates the line shape behavior of the experimental spectrum, with both large peak features narrowing slightly in comparison to the 3-pentanone results. This narrowing occurs because the methyl stretches no longer couple to the methylene modes. As a result, the methyl stretches of the different conformers appear at nearly the same frequency, decreasing the width of the composite peak. The peak centered at ~2890 cm^{-1} is the methyl symmetric vibrational stretching mode. The second peak at ~2955 cm^{-1} is the methyl asymmetric stretching mode. Again, there is a small peak in the experimental spectrum, tentatively assigned as a Fermi resonance, at 2982 cm^{-1}, which is not observed (or expected, as explained previously) in the theoretical spectrum.

The calculated and experimental spectra of 3-pentanone-d_4 in aqueous solution confirm that three of the peaks in the CH vibrational stretching region of 3-pentanone are due to modes with strong methyl vibration contributions, whereas one peak is dependent on the presence of the methylene vibrational stretching modes. Furthermore, the experimental spectrum of 3-pentanone-d_4 in an aqueous 0.275 M Na_2SO_4 solution reveals that the new peak observed at 2860 cm^{-1} in the spectrum of 3-pentanone in sulfate solution can be attributed to a methylene vibrational stretching mode.

The calculated spectrum of 3-pentanone in the carbonyl stretching region is shown in Figure 7. The carbonyl stretching modes of the various conformers all fall within 7 cm^{-1} of each other in energy, and their contributions to the spectral intensity per molecule are nearly equal. This results in a single feature in the composite spectrum. Nearly identical results were obtained for 3-pentanone-d_4. The single feature in the calculated spectrum is consistent with what is seen experimentally.

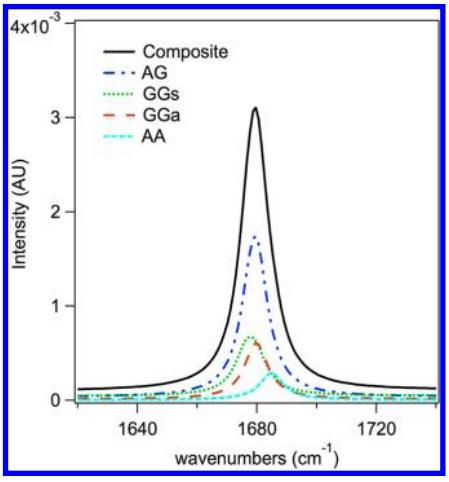

Figure 7. Calculated VSF spectrum in the carbonyl vibrational stretching region for 0.1 M 3-pentanone in water. The black trace represents the composite of the various conformers and their relative populations. The contributions from the individual conformers are also presented.

4.4. Computational Analysis of 3-Pentanone in Water and Na_2SO_4 Solution. Although the experiments provide information on the identity of the new methylene peak that appears upon addition of sodium sulfate to the solution, the cause underlying the appearance of the new peak is left unanswered. There are many scenarios one could use to explain the appearance of an additional peak in the CH region. Changes to the molecular species might occur in the presence of salts (i.e., changes to the enol/keto or diol/keto equilibrium). There could be mode shifting due to a direct interaction between the molecule and an ionic species or the electric field created by the layering of oppositely charged ions near the air−water interface. Finally, indirect changes induced by the electric field or changes in solvent structure at the surface could occur. These changes would affect the conformational and/or orientational distribution of the organic species at the air−water interface through coupling of the field with the molecular dipole or through changes in the water structure at the surface (induced by interactions with the electric field or other mechanisms).

Both changes to the molecular species and direct interaction with the molecule are inconsistent with the experimental results presented here. Increases in either the enol or diol forms of 3-pentanone would cause a decrease in the carbonyl stretching intensity, which was not observed. Barring that possibility, additional intensity due to the alcohol stretching modes would be expected. This was not observed and excludes changes to the molecular species present as a possible mechanism. Direct interaction was investigated using DFT calculations. Although VSF-active CH modes were shifted when 3-pentanone was calculated interacting with a sodium ion or a strong electric field, the shifting of the carbonyl stretching mode was always much stronger. No such shift was observed in the experimental spectra upon addition of sodium sulfate, also eliminating direct interaction mechanisms.

This leaves an indirect mechanism due to changes in orientation or conformation of the 3-pentanone molecules as the cause of the new peak in the 3-pentanone spectrum in the presence of Na_2SO_4. To investigate the validity of this hypothesis, the MD calculations involving 3-pentanone in water were compared to those of 3-pentanone in Na_2SO_4 solution with regard to orientation and conformation.

The conformational distribution of 3-pentanone in H_2O at the surface is negligibly different from the overall distribution because 3-pentanone rarely enters the bulk. At the surface, the AG conformer represents 42.3% of structures; GGs, 27.9%; GGa, 20.9%; and the AA conformation, 8.2%. With addition of Na_2SO_4, minor changes were observed. The largest of these changes was less than 0.5% of all structures. Such a small change led to insignificant changes in the overall spectrum.

Further comparison of MD calculations of 3-pentanone in water or in Na_2SO_4 solution revealed other seemingly minor changes in the behavior of 3-pentanone. Yet, there are two notable changes: First, the distribution of 3-pentanone molecules with respect to depth at the surface changes. Without the ions in solution, the 3-pentanone molecules exist in the topmost layers of water and slightly above the surface; when sulfate ions are present the 3-pentanone molecules adopt a more narrow distribution that does not extend as far above the water surface. The second change in the presence of Na_2SO_4 occurs in the distribution of angles that the carbonyl

adopts relative to the surface. The carbonyl angle distribution shifts slightly toward more shallow angles (more pointed toward the plane of the surface, less pointed toward bulk water). The number of 3-pentanone molecules with carbonyl angles between 120° and 160° is depleted, whereas the number of 3-pentanone molecules with carbonyl angles between 60° and 110° is enhanced in Na_2SO_4 solutions.

In fact, the depth relative to the surface and the orientation of the carbonyl group are strongly correlated at the air−water interface. The orientational distribution of the carbonyl bond as a function of depth is shown in Figure 8. When far above the surface (4−5 Å), the angular distribution is centered near 135°, corresponding to strongly pointing toward the bulk. As the molecules approach the water surface, the distribution shifts to shallower angles, eventually being centered around 90° (in the surface plane) when 2−3 Å below the surface. Below this depth, the majority of 3-pentanone molecules orient with the carbonyl pointing out of the bulk. Although this shows a strong connection between depth and orientation and the addition of Na_2SO_4 shows changes in the orientation and density profile of 3-pentanone, it is unclear whether the reorientation is due to the 3-pentanone molecules being held more tightly to the surface or whether the 3-pentanone moves closer to the surface as a result of being reoriented. It also remains to be seen if the reorientation can explain the spectral changes observed experimentally.

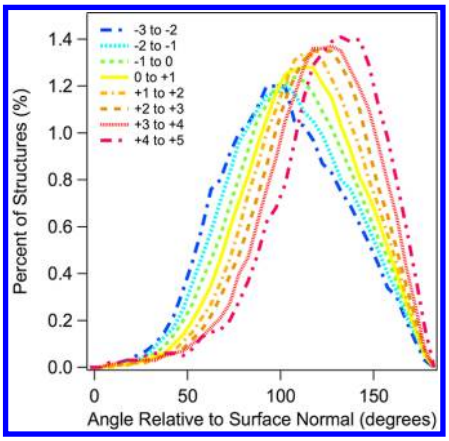

Figure 8. Calculated distribution of the carbonyl angle relative to the surface normal at various depths. An angle of 90° relative to the surface normal corresponds to the C═O in plane with the water surface.

To investigate the impact of the reorientation of 3-pentanone on the VSF spectrum, the spectrum was calculated with the carbonyl oriented at several angles. This involves rotation of the structures used to calculate the spectrum in Figure 6 about the axis parallel to the plane of the water surface and perpendicular to the carbonyl bond to reach the desired angle. In Figure 9, the VSF spectra were calculated for the carbonyl at angles of 90°, 105°, 120°, and 135°. An angle of 90° corresponds to the carbonyl in the plane of the interface, whereas 135° corresponds to the carbonyl pointing 45° into the bulk. As the angle decreases, a new peak arises at ∼2865 cm^{-1}, unique to the AG conformer. The 2865 cm^{-1} peak is the symmetric stretching mode of the methylene moiety in the A formation. This mode is unique to the AG conformer, as the other conformers lack the methylene group in the A formation (GGa, GGs) or the methylene symmetric stretching mode is coupled to other CH vibrational modes and the resulting mode is blue-shifted. For example, the methylene symmetric stretching mode of the AA conformation appears at approximately 2880 cm^{-1}. The reorientation observed in the MD results and the additional peak that appears in the DFT spectra when such a reorientation is taken into account agree with the experimental results, confirming that reorientation is the likely cause of the changes in the CH stretching region of the spectrum.

4.5. Evidence That Na_2SO_4 Induces Reorientation of 3-Pentanone at the Interface. Reorientation of 3-pentanone provides an explanation for the appearance of the CH peak that appears with the addition of Na_2SO_4 to the solution. Still, it is unclear how the reorientation is large enough to give rise to the new CH peak while leaving the CO stretching peak relatively unchanged. To investigate how the spectrum is expected to change in both the CH and CO stretching regions with the proposed reorientation, the *YYZ* second-order susceptibility tensor element was calculated as a function of orientational angle. This was done for the carbonyl stretching mode and the methylene symmetric stretching mode of the AG conformer. The resulting behavior is shown in Figure 10. Also shown is an approximate representation of the change in the number density (3-pentanone number density in Na_2SO_4 solution minus that in water) as a function of orientational angle. To calculate the SSP VSF intensity, one first forms the product of the number density and the *YYZ* second-order tensor element. This product is integrated over all angles, and the result is squared to give the VSF intensity. For the tensor element of the carbonyl stretching mode, minima appear at 0° and 180° relative to the surface normal. Maxima occur near 55° and 125° with zero crossing at 90°. The *YYZ* second-order susceptibility tensor element component of the methylene stretching mode has a maximum near 55° and passes through zero near 130°.

Considering the changes in the distribution of carbonyl pointing angles obtained from the MD calculations, we can predict how the intensities of the VSF spectrum will be affected. First, we focused on the methylene stretching mode of the AG conformer. The distribution of carbonyl angles of 3-pentanone in water (not shown) is at a maximum near where the susceptibility tensor element of the methylene stretching mode switches signs. Assuming a nearly symmetric distribution of the carbonyl angles, positive contributions to the integrand (mentioned above) at angles less than 130° and negative contributions at angles greater than 130° nearly cancel out. The integrand and its square are both approximately zero; hence, the VSF intensity is very weak. This leads to little or no measurable signal of the methylene symmetric vibrational stretching mode in the VSF spectrum in solutions without Na_2SO_4. However, the MD results for 3-pentanone in Na_2SO_4 solution show a change in the number-density-versus-bond-angle distribution (i.e., the green curve in Figure 10 is not zero). With Na_2SO_4, more molecules are in the 90° range, and fewer are in the 150° range. The consequence of this change is that the contributions to the integrand used to calculate the VSF intensity no longer cancel. This can be visualized by taking the product of the change in the number density and the *YYZ* component of the methylene stretching mode susceptibility tensor. Over nearly the entire range of angles, this product retains the same sign. When integrated and squared, the result will be large considering the number density change involved. With positive contributions of the susceptibility tensor element getting a boost (positive change in number density) and negative contributions being depleted (negative change in

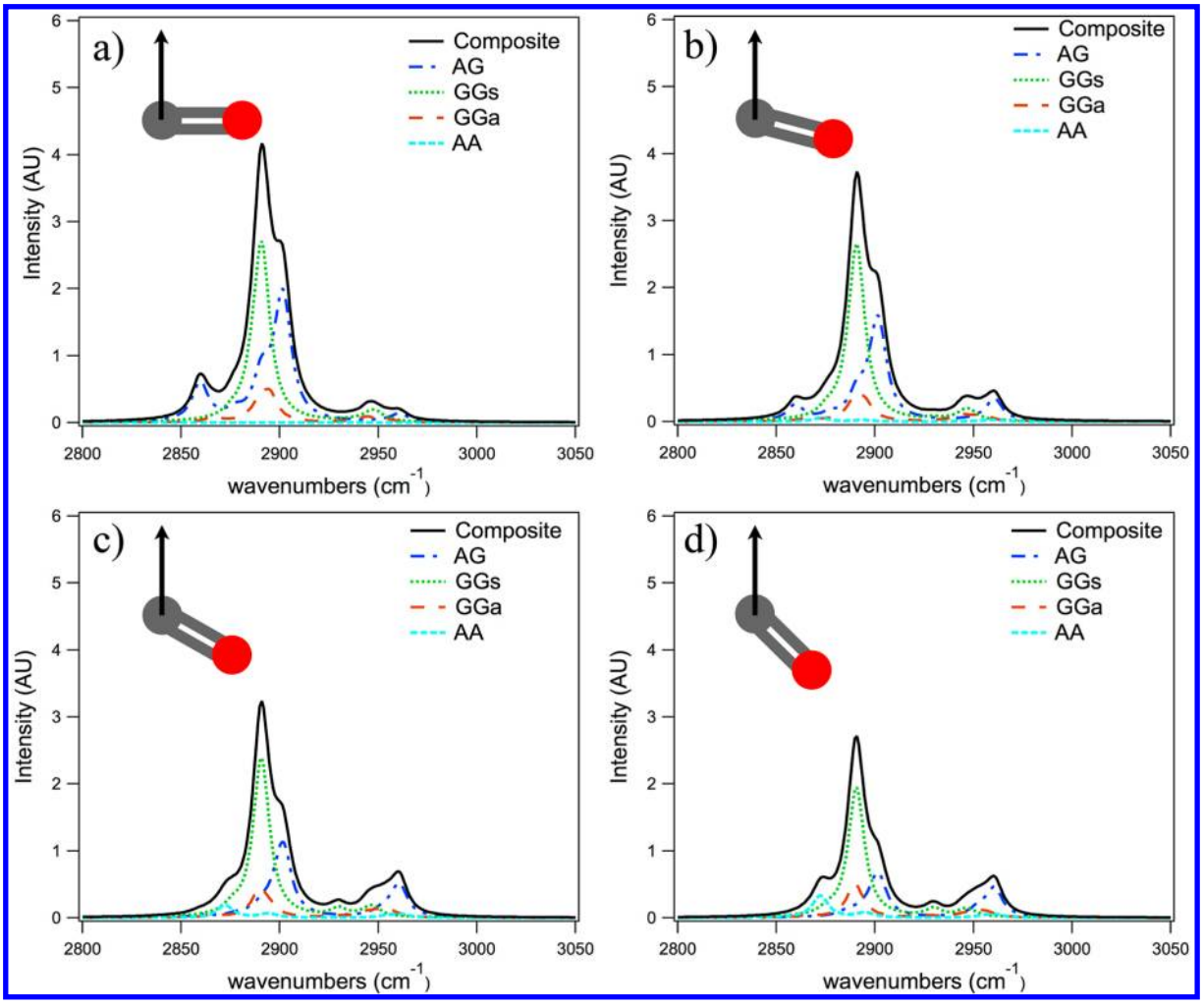

Figure 9. Calculated spectra of 3-pentanone in the CH vibrational mode region at various angles of the carbonyl group: (a) 90° (carbonyl in plane with the surface), (b) 105°, (c) 120°, and (d) 135°. The black trace is a composite of the individual conformers, and the contributions from each conformer are also presented.

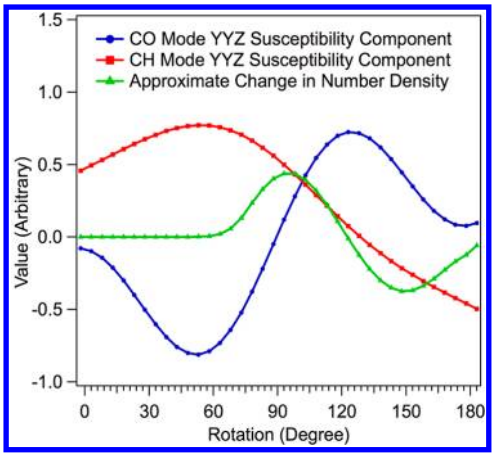

Figure 10. Second-order susceptibility tensor *YYZ* components for the methylene symmetric stretch (red squares) and carbonyl stretch (blue circles) of the AG conformer as a function of the angle between the carbonyl bond and the *z* axis. Also shown is the approximate change in the number density of molecules at the bond angle indicated in the distribution of carbonyls at the surface when sodium sulfate is added to molecular dynamics calculations (green triangles).

number density), a peak at 2860 cm^{-1} is expected to appear in the VSF spectrum.

For the carbonyl stretching mode, the observed experimental peak changes minimally with the addition of sodium sulfate. Using the same analysis as for the methylene peak at 2860 cm^{-1}, we expect both depletion and enhancement of the signal due to orientation changes. The integrated product of the CO stretching mode *YYZ* susceptibility with the number density of aqueous 3-pentanone is strongly positive. Analysis of the product using the number density change allows the effect of addition of Na_2SO_4 to be predicted. Depletion of the signal is caused by a reduction of orientations with C═O angles greater than 125° and a further decrease in signal resulting from orientations less than 90°. Enhancement of VSF signal is expected from increasing contributions of the *YYZ* susceptibility tensor element between 90° and 125°. These competing factors can lead to the intensity of the carbonyl stretching mode remaining nearly constant over small changes in orientation while the methylene stretching mode undergoes very large changes in intensity with the same relatively minor changes in the orientational distribution.

Although the behavior of 3-pentanone at the interface is different in the presence of sulfate ions, the interaction between the ions and the other molecules is more difficult to elucidate.

dx.doi.org/10.1021/jp408188x | J. Phys. Chem. A 2013, 117, 11514−11527

The role of ions at the interface has been widely studied and debated.[21,28−30,35,36,38,39,41,68,86,93,95,98−107] Initially, it was believed that the ions were excluded from the interface; however, it has been shown that some ions do permeate the interface and that ions impact the structure of water molecules at the interface. Larger more polarizable ions, such as sulfate, are forced deeper into the bulk water for solvation. The separation of ions at the interface creates an electric field, which has been studied previously.[20,57,101,108−110] New advances in the realm of phase-sensitive sum frequency generation have provided new insight into the electric field and orientation of salts at the air−water interface. These studies have shown that the orientation of Na_2SO_4 is opposite that of NaCl or Na_2CO_3.[40] Furthermore, studies have suggested that the electric field produced by Na_2SO_4 is stronger than that produced by other salts.[41] The lack of change in the VSF spectra of 3-pentanone in NaCl or Na_2CO_3 solutions indicates that the presence of these ions does not cause significant reorientation, whereas the Na_2SO_4 solution does cause reorientation of 3-pentanone molecules. These ions also produce a salting-out effect, which cannot be ignored, but does not explain the observed spectral differences of 3-pentanone in Na_2SO_4, Na_2CO_3, and NaCl solutions. The most consistent explanation of the different behavior in Na_2SO_4 solutions is that the dipole of the carbonyl group on the 3-pentanone molecules reorients in the presence of an electric field. Both the direction of the Na_2SO_4 field and its larger magnitude are necessary to cause the changes in the 3-pentanone VSF spectrum.

5. CONCLUSIONS

Given the prevalence of ketones in the atmosphere, understanding their molecular behavior at aqueous interfaces where they often reside is important to furthering our knowledge of atmospheric chemistry at aerosol surfaces. In this study, we have combined spectroscopic characterization and computer simulations to provide the most detailed picture to date of adsorption of a ketone, specifically 3-pentanone, to the surface of aqueous salt solutions. We found that the adsorption of 3-pentanone at the vapor−water boundary layer is most affected by the presence of sulfate ions in the aqueous phase. The results demonstrate that sodium sulfate causes 3-pentanone to reorient, reside deeper in the interface, and occupy a smaller distribution of depths relative to a neat water surface or solutions containing NaCl or Na_2CO_3. The depth of 3-pentanone is strongly correlated with the distribution of carbonyl angles relative to the water surface. In the presence of sodium sulfate in the aqueous phase, the angle of the 3-pentanone carbonyl relative to the surface is shallower, approaching planarity with the water surface. Analysis of the carbonyl and OH stretching regions eliminates all but an indirect interaction mechanism in which coupling of polar groups in the interfacial layer to the field created by the charge separation of ionic species results in altered behavior. Whereas the electric field due to sodium and sulfate ions has the direction and magnitude to cause an observable reorientation, the electric fields for sodium chloride and sodium carbonate have an improper direction and/or insufficient intensity to induce an observable effect. In atmospheric waters, the presence of sulfate is common and likely to cause a similar effect, thus causing polar organic molecules to reside deeper in the interface. Although we are able to observe this behavior for 3-pentanone only because of its unique properties, we expect this to be a general phenomenon.

AUTHOR INFORMATION

Corresponding Author

*Tel.: 541-346-4635. Fax: 541-346-5859. E-mail: richmond@uoregon.edu.

Notes

The authors declare no competing financial interest.

ACKNOWLEDGMENTS

Financial support for this research was provided by the National Science Foundation (NSF-CHE-1051215). We also acknowledge assistance with the manuscript from Laura McWilliams (University of Oregon) and Prof. Fred Moore (Whitman College) and assistance with experimental design from Dr. Larry Scatena (University of Oregon).

REFERENCES

(1) Jimenez, J. L.; Canagaratna, M. R.; Donahue, N. M.; Prevot, A. S. H.; Zhang, Q.; Kroll, J. H.; DeCarlo, P. F.; Allan, J. D.; Coe, H.; Ng, N. L.; et al. Evolution of Organic Aerosols in the Atmosphere. *Science* **2009**, *326*, 1525−1529.

(2) IPCC. *Climate Change: The Physical Science Basis - Contribution of Working Group I to the Fourth Assessment Report of the Intergovernmental Panel on Climate Change*; Cambridge University Press: Cambridge, U.K., 2007.

(3) Ebben, C. J.; Shrestha, M.; Martinez, I. S.; Corrigan, A. L.; Frossard, A. A.; Song, W. W.; Worton, D. R.; Petaja, T.; Williams, J.; Russell, L. M.; Kulmala, M.; Goldstein, A. H.; Artaxo, P.; Martin, S. T.; Thomson, R. J.; Geiger, F. M. Organic Constituents on the Surfaces of Aerosol Particles from Southern Finland, Amazonia, and California Studied by Vibrational Sum Frequency Generation. *J. Phys. Chem. A* **2012**, *116*, 8271−8290.

(4) Ravishankara, A. R. Heterogeneous and Multiphase Chemistry in the Troposphere. *Science* **1997**, *276*, 1058−1065.

(5) Kolb, C. E.; Worsnop, D. R. Chemistry and Composition of Atmospheric Aerosol Particles. *Annu. Rev. Phys. Chem.* **2012**, *63*, 471−491.

(6) Kroll, J. H.; Ng, N. L.; Murphy, S. M.; Varutbangkul, V.; Flagan, R. C.; Seinfeld, J. H. Chamber Studies of Secondary Organic Aerosol Growth by Reactive Uptake of Simple Carbonyl Compounds. *J. Geophys. Res.* **2005**, *110*, D23207.

(7) Volkamer, R.; Martini, F. S.; Molina, L. T.; Salcedo, D.; Jimenez, J. L.; Molina, M. J. A Missing Sink for Gas-Phase Glyoxal in Mexico City: Formation of Secondary Organic Aerosol. *Geophys. Res. Lett.* **2007**, *34*, L19807.

(8) Galloway, J. N.; Likens, G. E.; Keene, W. C.; Miller, J. M. The Composition of Precipitation in Remote Areas of the World. *J. Geophys. Res.* **1982**, *87*, 8771−8786.

(9) Grosjean, D.; Wright, B. Carbonyls in Urban Fog, Ice Fog, Cloudwater and Rainwater. *Atmos. Environ.* **1983**, *17*, 2093−2096.

(10) Igawa, M.; Munger, J. W.; Hoffmann, M. R. Analysis of Aldehydes in Cloud Samples and Fogwater Samples by HPLC with a Postcolumn Reaction Detector. *Environ. Sci. Technol.* **1989**, *23*, 556−561.

(11) Jacob, D. J.; Waldman, J. M.; Munger, J. W.; Hoffmann, M. R. Chemical Composition of Fogwater Collected along the California Coast. *Environ. Sci. Technol.* **1985**, *19*, 730−736.

(12) Kawamura, K.; Kaplan, I. R. Organic Compounds in the Rainwater of Los Angeles. *Environ. Sci. Technol.* **1983**, *17*, 497−501.

(13) Likens, G. E.; Edgerton, E. S.; Galloway, J. N. The Composition and Deposition of Organic Carbon in Precipitation. *Tellus* **1983**, *35B*, 16−24.

(14) Chen, H.; Gan, W.; Wu, B. H.; Wut, D.; Guo, Y.; Wang, H. F. Determination of Structure and Energetics for Gibbs Surface

Adsorption Layers of Binary Liquid Mixture 1. Acetone + Water. *J. Phys. Chem. B* **2005**, *109*, 8053−8063.
(15) Johnson, C. M.; Tyrode, E.; Leygraf, C. Atmospheric Corrosion of Zinc by Organic Constituents I. The Role of the Zinc/Water and Water/Air Interfaces Studied by Infrared Reflection/Absorption Spectroscopy and Vibrational Sum Frequency Spectroscopy. *J. Electrochem. Soc.* **2006**, *153*, B113−B120.
(16) Ota, S. T.; Richmond, G. L. Uptake of SO_2 to Aqueous Formaldehyde Surfaces. *J. Am. Chem. Soc.* **2012**, *134*, 9967−9977.
(17) Yeh, Y. L.; Zhang, C.; Held, H.; Mebel, A. M.; Wei, X.; Lin, S. H.; Shen, Y. R. Structure of the Acetone Liquid/Vapor Interface. *J. Chem. Phys.* **2001**, *114*, 1837−1843.
(18) Tang, C. Y.; Allen, H. C. Ionic Binding of Na^+ versus K^+ to the Carboxylic Acid Headgroup of Palmitic Acid Monolayers Studied by Vibrational Sum Frequency Generation Spectroscopy. *J. Phys. Chem. A* **2009**, *113*, 7383−7393.
(19) Tang, C. Y.; Huang, Z.; Allen, H. C. Binding of Mg^{2+} and Ca^{2+} to Palmitic Acid and Deprotonation of the COOH Headgroup Studied by Vibrational Sum Frequency Generation Spectroscopy. *J. Phys. Chem. B* **2010**, *114*, 17068−17076.
(20) Tang, C. Y.; Huang, Z.; Allen, H. C. Interfacial Water Structure and Effects of Mg^{2+} and Ca^{2+} Binding to the COOH Headgroup of a Palmitic Acid Monolayer Studied by Sum Frequency Spectroscopy. *J. Phys. Chem. B* **2011**, *115*, 34−40.
(21) Soule, M. C. K.; Blower, P. G.; Richmond, G. L. Effects of Atmospherically Important Solvated Ions on Organic Acid Adsorption at the Surface of Aqueous Solutions. *J. Phys. Chem. B* **2007**, *111*, 13703−13713.
(22) Finlayson-Pitts, B.; Pitts, J., Jr. *Chemistry of the Upper and Lower Atmosphere*; Academic Press: New York, 2000.
(23) Charlson, R. J.; Schwartz, S. E.; Hales, J. M.; Cess, R. D.; Coakley, J. A.; Hansen, J. E.; Hofmann, D. J. Climate Forcing by Anthropogenic Aerosols. *Science* **1992**, *255*, 423−430.
(24) Tarbuck, T. L.; Richmond, G. L. Adsorption and Reaction of CO_2 and SO_2 at a Water Surface. *J. Am. Chem. Soc.* **2006**, *128*, 3256−3267.
(25) Donaldson, D. J.; Guest, J. A.; Goh, M. C. Evidence for Adsorbed SO_2 at the Aqueous Air Interface. *J. Phys. Chem.* **1995**, *99*, 9313−9315.
(26) Ghosal, S.; Hemminger, J. C.; Bluhm, H.; Mun, B. S.; Hebenstreit, E. L. D.; Ketteler, G.; Ogletree, D. F.; Requejo, F. G.; Salmeron, M. Electron Spectroscopy of Aqueous Solution Interfaces Reveals Surface Enhancement of Halides. *Science* **2005**, *307*, 563−566.
(27) Gurau, M. C.; Lim, S. M.; Castellana, E. T.; Albertorio, F.; Kataoka, S.; Cremer, P. S. On the Mechanism of the Hofmeister Effect. *J. Am. Chem. Soc.* **2004**, *126*, 10522−10523.
(28) Jungwirth, P.; Tobias, D. J. Ions at the Air/Water Interface. *J. Phys. Chem. B* **2002**, *106*, 6361−6373.
(29) Knipping, E. M.; Lakin, M. J.; Foster, K. L.; Jungwirth, P.; Tobias, D. J.; Gerber, R. B.; Dabdub, D.; Finlayson-Pitts, B. J. Experiments and Simulations of Ion-Enhanced Interfacial Chemistry on Aqueous NaCl Aerosols. *Science* **2000**, *288*, 301−306.
(30) Liu, D. F.; Ma, G.; Levering, L. M.; Allen, H. C. Vibrational Spectroscopy of Aqueous Sodium Halide Solutions and Air−Liquid Interfaces: Observation of Increased Interfacial Depth. *J. Phys. Chem. B* **2004**, *108*, 2252−2260.
(31) Jubb, A. M.; Allen, H. C. Bisulfate Dehydration at Air/Solution Interfaces Probed by Vibrational Sum Frequency Generation Spectroscopy. *J. Phys. Chem. C* **2012**, *116*, 13161−13168.
(32) Gopalakrishnan, S.; Liu, D. F.; Allen, H. C.; Kuo, M.; Shultz, M. J. Vibrational Spectroscopic Studies of Aqueous Interfaces: Salts, Acids, Bases, and Nanodrops. *Chem. Rev.* **2006**, *106*, 1155−1175.
(33) Ishiyama, T.; Morita, A.; Miyamae, T. Surface Structure of Sulfuric Acid Solution Relevant to Sulfate Aerosol: Molecular Dynamics Simulation Combined with Sum Frequency Generation Measurement. *Phys. Chem. Chem. Phys.* **2011**, *13*, 20965−20973.
(34) Jubb, A. M.; Hua, W.; Allen, H. C. Environmental Chemistry at Vapor/Water Interfaces: Insights from Vibrational Sum Frequency Generation Spectroscopy. *Annu. Rev. Phys. Chem.* **2012**, *63*, 107−130.
(35) Mucha, M.; Frigato, T.; Levering, L. M.; Allen, H. C.; Tobias, D. J.; Dang, L. X.; Jungwirth, P. Unified Molecular Picture of the Surfaces of Aqueous Acid, Base, and Salt Solutions. *J. Phys. Chem. B* **2005**, *109*, 7617−7623.
(36) Pegram, L. M.; Record, M. T., Jr. Partitioning of Atmospherically Relevant Ions Between Bulk Water and the Water/Vapor Interface. *Proc. Natl. Acad. Sci. U.S.A.* **2006**, *103*, 14278−14281.
(37) Sahu, K.; McNeill, V. F.; Eisenthal, K. B. Effect of Salt on the Adsorption Affinity of an Aromatic Carbonyl Molecule to the Air−Aqueous Interface: Insight for Aqueous Environmental Interfaces. *J. Phys. Chem. C* **2010**, *114*, 18258−18262.
(38) Shultz, M. J.; Schnitzer, C.; Simonelli, D.; Baldelli, S. Sum Frequency Generation Spectroscopy of the Aqueous Interface: Ionic and Soluble Molecular Solutions. *Int. Rev. Phys. Chem.* **2000**, *19*, 123−153.
(39) Raymond, E. A.; Richmond, G. L. Probing the Molecular Structure and Bonding of the Surface of Aqueous Salt Solutions. *J. Phys. Chem. B* **2004**, *108*, 5051−5059.
(40) Hua, W.; Jubb, A. M.; Allen, H. C. Electric Field Reversal of Na_2SO_4, $(NH_4)_2SO_4$, and Na_2CO_3 Relative to $CaCl_2$ and NaCl at the Air/Aqueous Interface Revealed by Heterodyne Detected Phase-Sensitive Sum Frequency. *J. Phys. Chem. Lett.* **2011**, *2*, 2515−2520.
(41) Tian, C.; Byrnes, S. J.; Han, H.-L.; Shen, Y. R. Surface Propensities of Atmospherically Relevant Ions in Salt Solutions Revealed by Phase-Sensitive Sum Frequency Vibrational Spectroscopy. *J. Phys. Chem. Lett.* **2011**, *2*, 1946−1949.
(42) Green, A. J.; Perry, A.; Moore, P. B.; Space, B. A Theoretical Study of the Sum Frequency Vibrational Spectroscopy of the Carbon Tetrachloride/Water Interface. *J. Phys.: Condens. Matter* **2012**, *24*, 124108.
(43) Ishiyama, T.; Morita, A. Molecular Dynamics Simulation of Sum Frequency Generation Spectra of Aqueous Sulfuric Acid Solution. *J. Phys. Chem. C* **2011**, *115*, 13704−13716.
(44) Ishiyama, T.; Takahashi, H.; Morita, A. Vibrational Spectrum at a Water Surface: A Hybrid Quantum Mechanics/Molecular Mechanics Molecular Dynamics Approach. *J. Phys.: Condens. Matter* **2012**, *24*, 124107.
(45) Morita, A.; Hynes, J. T. A Theoretical Analysis of the Sum Frequency Generation Spectrum of the Water Surface. *Chem. Phys.* **2000**, *258*, 371−390.
(46) Morita, A.; Ishiyama, T. Recent Progress in Theoretical Analysis of Vibrational Sum Frequency Generation Spectroscopy. *Phys. Chem. Chem. Phys.* **2008**, *10*, 5801−5816.
(47) Sulpizi, M.; Salanne, M.; Sprik, M.; Gaigeot, M.-P. Vibrational Sum Frequency Generation Spectroscopy of the Water Liquid−Vapor Interface from Density Functional Theory-Based Molecular Dynamics Simulations. *J. Phys. Chem. Lett.* **2013**, *4*, 83−87.
(48) Buch, V.; Tarbuck, T.; Richmond, G. L.; Groenzin, H.; Li, I.; Shultz, M. J. Sum Frequency Generation Surface Spectra of Ice, Water, and Acid Solution Investigated by an Exciton Model. *J. Chem. Phys.* **2007**, *127*, 204710.
(49) Walker, D. S.; Hore, D. K.; Richmond, G. L. Understanding the Population, Coordination, and Orientation of Water Species Contributing to the Nonlinear Optical Spectroscopy of the Vapor-Water Interface through Molecular Dynamics Simulations. *J. Phys. Chem. B* **2006**, *110*, 20451−20459.
(50) Walker, D. S.; Moore, F. G.; Richmond, G. L. Vibrational Sum Frequency Spectroscopy and Molecular Dynamics Simulation of the Carbon Tetrachloride−Water and 1,2-Dichloroethane−Water Interfaces. *J. Phys. Chem. C* **2007**, *111*, 6103−6112.
(51) Walker, D. S.; Richmond, G. L. Depth Profiling of Water Molecules at the Liquid−Liquid Interface Using a Combined Surface Vibrational Spectroscopy and Molecular Dynamics Approach. *J. Am. Chem. Soc.* **2007**, *129*, 9446−9451.
(52) Walker, D. S.; Richmond, G. L. Understanding the Effects of Hydrogen Bonding at the Vapor−Water Interface: Vibrational Sum Frequency Spectroscopy of H_2O/HOD/D_2O Mixtures Studied Using Molecular Dynamics Simulations. *J. Phys. Chem. C* **2007**, *111*, 8321−8330.

(53) Blower, P. G.; Ota, S. T.; Valley, N. A.; Wood, S. R.; Richmond, G. L. Sink or Surf: Atmospheric Implications for Succinic Acid at Aqueous Surfaces. *J. Phys. Chem. A* **2013**, *117*, 7887−7903.
(54) Bain, C. D. Sum-Frequency Vibrational Spectroscopy of the Solid−Liquid Interface. *J. Chem. Soc., Faraday Trans.* **1995**, *91*, 1281−1296.
(55) Bloember, N. Second Harmonic Reflected Light. *Opt. Acta* **1966**, *13*, 311−322.
(56) Buck, M.; Himmelhaus, M. Vibrational Spectroscopy of Interfaces by Infrared−Visible Sum Frequency Generation. *J. Vac. Sci. Technol.* **2001**, *A19*, 2717−2736.
(57) Fourkas, J. T.; Walker, R. A.; Can, S. Z.; Gershgoren, E. Effects of Reorientation in Vibrational Sum-Frequency Spectroscopy. *J. Phys. Chem. C* **2007**, *111*, 8902−8915.
(58) Hemminger, J. C. Heterogeneous Chemistry in the Troposphere: A Modern Surface Chemistry Approach to the Study of Fundamental Processes. *Int. Rev. Phys. Chem.* **1999**, *18*, 387−417.
(59) Hirose, C.; Akamatsu, N.; Domen, K. Formulas for the Analysis of the Surface SFG Spectrum and Transformation Coefficients of Cartesian SFG Tensor Components. *Appl. Spectrosc.* **1992**, *46*, 1051−1072.
(60) Ishibashi, T. A.; Onishi, H. Multiplex Infrared-Visible Sum-Frequency Spectrometer with a Phase-Conjugated Pulse Mixing Device for Narrow-Bandwidth Visible Probe Generation. *Appl. Spectrosc.* **2002**, *56*, 1298−1302.
(61) Ji, N.; Ostroverkhov, V.; Belkin, M.; Shiu, Y.-J.; Shen, Y.-R. Toward Chiral Sum-Frequency Spectroscopy. *J. Am. Chem. Soc.* **2006**, *128*, 8845−8848.
(62) Lambert, A. G.; Davies, P. B.; Neivandt, D. J. Implementing the Theory of Sum Frequency Generation Vibrational Spectroscopy: A Tutorial Review. *Appl. Spectrosc. Rev.* **2005**, *40*, 103−145.
(63) Lobau, J.; Wolfrum, K. Sum-Frequency Spectroscopy in Total Internal Reflection Geometry: Signal Enhancement and Access to Molecular Properties. *J. Opt. Soc. Am. B* **1997**, *14*, 2505−2512.
(64) McGall, S. J.; Davies, P. B.; Neivandt, D. J. Interference Effects in Sum Frequency Vibrational Spectra of Thin Polymer Films: An Experimental and Modeling Investigation. *J. Phys. Chem. B* **2004**, *108*, 16030−16039.
(65) Miranda, P. B.; Shen, Y. R. Liquid Interfaces: A Study by Sum-Frequency Vibrational Spectroscopy. *J. Phys. Chem. B* **1999**, *103*, 3292−3307.
(66) Ostroverkhov, V.; Waychunas, G. A.; Shen, Y. R. New Information on Water Interfacial Structure Revealed by Phase-Sensitive Surface Spectroscopy. *Phys. Rev. Lett.* **2005**, *94*, 046102.
(67) Rao, Y.; Song, D.; Turro, N. J.; Eisenthal, K. B. Orientational Motions of Vibrational Chromophores in Molecules at the Air/Water Interface with Time-Resolved Sum Frequency Generation. *J. Phys. Chem. B* **2008**, *112*, 13572−13576.
(68) Richmond, G. L. Molecular Bonding and Interactions at Aqueous Surfaces as Probed by Vibrational Sum Frequency Spectroscopy. *Chem. Rev.* **2002**, *102*, 2693−2724.
(69) Shen, Y. R. Surface Properties Probed by Second-Harmonic and Sum-Frequency Generation. *Nature* **1989**, *337*, 519−525.
(70) Shen, Y. R. Exploring New Opportunities with Sum-Frequency Nonlinear Optical Spectroscopy. *Pure Appl. Chem.* **2001**, *73*, 1589−1598.
(71) Shen, Y. R.; Ostroverkhov, V. Sum-Frequency Vibrational Spectroscopy on Water Interfaces: Polar Orientation of Water Molecules at Interfaces. *Chem. Rev.* **2006**, *106*, 1140−1154.
(72) Vidal, F.; Tadjeddine, A. Sum-Frequency Generation Spectroscopy of Interfaces. *Rep. Prog. Phys.* **2005**, *68*, 1095−1127.
(73) Zhu, X. D.; Suhr, H.; Shen, Y. R. Surface Vibrational Spectroscopy by Infrared-Visible Sum Frequency Generation. *Phys. Rev. B* **1987**, *35*, 3047−3050.
(74) Bain, C. D.; Davies, P. B.; Ong, T. H.; Ward, R. N.; Brown, M. A. Quantitative Analysis of Monolayer Composition by Sum-Frequency Vibrational Spectroscopy. *Langmuir* **1991**, *7*, 1563−1566.
(75) Soule, M. C. K.; Blower, P. G.; Richmond, G. L. Nonlinear Vibrational Spectroscopic Studies of the Adsorption and Speciation of Nitric Acid at the Vapor/Acid Solution Interface. *J. Phys. Chem. A* **2007**, *111*, 3349−3357.
(76) Blower, P. G.; Shamay, E.; Kringle, L.; Ota, S. T.; Richmond, G. L. Surface Behavior of Malonic Acid Adsorption at the Air/Water Interface. *J. Phys. Chem. A* **2013**, *117*, 2529−2542.
(77) Allen, H. C.; Raymond, E. A.; Richmond, G. L. Surface Structural Studies of Methanesulfonic Acid at Air/Aqueous Solution Interfaces Using Vibrational Sum Frequency Spectroscopy. *J. Phys. Chem. A* **2001**, *105*, 1649−1655.
(78) Gragson, D. E.; Alavi, D. S.; Richmond, G. L. Tunable Picosecond Infrared Laser System Based on Parametric Amplification in KTP with a Ti:Sapphire Amplifier. *Opt. Lett.* **1995**, *20*, 1991−1993.
(79) Gragson, D. E.; McCarty, B. M.; Richmond, G. L.; Alavi, D. S. High-Power Broadly Tunable Picosecond IR Laser System for Use in Nonlinear Spectroscopic Applications. *J. Opt. Soc. Am. B* **1996**, *13*, 2075−2083.
(80) Case, D. A.; Darden, T. A.; Cheatham, T. E., III; Simmerling, C. L.; Wang, J.; Duke, R. E.; Luo, R.; Walker, R. C.; Zhang, W.; Merz, K. M.; Roberts, B.; Hayik, S.; Roitberg, A.; Seabra, G.; Swails, J.; Goetz, A. W.; Kolossváry, I.; Wong, K. F.; Paesani, F.; Vanicek, J.; Wolf, R. M.; Liu, J.; Wu, X.; Brozell, S. R.; Steinbrecher, T.; Gohlke, H.; Cai, Q.; Ye, X.; Wang, J.; Hsieh, M.-J.; Cui, G.; Roe, D. R.; Mathews, D. H.; Seetin, M. G.; Salomon-Ferrer, R.; Sagui, C.; Babin, V.; Luchko, T.; Gusarov, S.; Kovalenko, A.; Kollman, P. A. *AMBER 12*; University of California: San Francisco, CA, 2012.
(81) Martinez, L.; Andrade, R.; Birgin, E.; Martinez, J. PACKMOL: A Package for Building Initial Configurations for Molecular Dynamics Simulations. *J. Comput. Chem.* **2009**, *30*, 2157−2164.
(82) Caldwell, J. W.; Kollman, P. A. Structure and Properties of Neat Liquids Using Nonadditive Molecular Dynamics: Water, Methanol, and *N*-Methylacetamide. *J. Phys. Chem.* **1995**, *99*, 6208−6219.
(83) Case, D. A.; Cheatham, T. E.; Darden, T.; Gohlke, H.; Luo, R.; Merz, K. M.; Onufriev, A.; Simmerling, C.; Wang, B.; Woods, R. J. The Amber Biomolecular Simulation Programs. *J. Comput. Chem.* **2005**, *26*, 1668−1688.
(84) Jungwirth, P.; Curtis, J. E.; Tobias, D. J. Polarizability and Aqueous Solvation of the Sulfate Dianion. *Chem. Phys. Lett.* **2003**, *367*, 704−710.
(85) Valiev, M.; Bylaska, E. J.; Govind, N.; Koawlski, K.; Straatsma, T. P.; Dam, H. J. J.; Wang, D.; Nieplocha, J.; Apra, E.; Windus, T. L.; de Jong, W. NWChem: A Comprehensive and Scalable Open-Source Solution for Large Scale Molecular Simulations. *Comput. Phys. Commun.* **2010**, *181*, 1477−1489.
(86) Raymond, E. A.; Tarbuck, T. L.; Brown, M. G.; Richmond, G. L. Hydrogen-Bonding Interactions at the Vapor/Water Interfaces Investigated by Vibrational Sum-Frequency Spectroscopy of HOD/H_2O/D_2O Mixtures and Molecular Dynamics Simulations. *J. Phys. Chem. B* **2003**, *107*, 546−556.
(87) Stanners, C. D.; Du, Q.; Chin, R. P.; Cremer, P.; Somorjai, G. A.; Shen, Y. R. Polar Ordering at the Liquid−Vapor Interface of *n*-Alcohols (C_1−C_8). *Chem. Phys. Lett.* **1995**, *232*, 407−413.
(88) Tarbuck, T. L.; Richmond, G. L. Adsorptions of Organosulfur Species at Aqueous Surfaces: Molecular Bonding and Orientation. *J. Phys. Chem. B* **2005**, *109*, 20868−20877.
(89) Bakker, H. J.; Skinner, J. L. Vibrational Spectroscopy as a Probe of Structure and Dynamics in Liquid Water. *Chem. Rev.* **2010**, *110*, 1498−1517.
(90) Buch, V. Molecular Structure and OH-Stretch Spectra of Liquid Water Surface. *J. Phys. Chem. B* **2005**, *109*, 17771−17774.
(91) Dang, L. X.; Chang, T. M. Molecular Dynamics Study of Water Clusters, Liquid, and Liquid−Vapor Interface of Water with Many-Body Potentials. *J. Chem. Phys.* **1997**, *106*, 8149−8159.
(92) Raymond, E. A.; Tarbuck, T. L.; Richmond, G. L. Isotopic Dilution Studies of the Vapor/Water Interface as Investigated by Vibrational Sum-Frequency Spectroscopy. *J. Phys. Chem. B* **2002**, *106*, 2817−2820.
(93) Tarbuck, T. L.; Ota, S. T.; Richmond, G. L. Spectroscopic Studies of Solvated Hydrogen and Hydroxide Ions at Aqueous Surfaces. *J. Am. Chem. Soc.* **2006**, *128*, 14519−14527.

(94) Jubb, A. M.; Hua, W.; Allen, H. C. Organization of Water and Atmospherically Relevant Ions and Solutes: Vibrational Sum Frequency Spectroscopy at the Vapor/Liquid and Liquid/Solid Interfaces. *Acc. Chem. Res.* **2012**, *45*, 110−119.
(95) Jungwirth, P.; Tobias, D. J. Molecular Structure of Salt Solutions: A New View of the Interface with Implications for Heterogeneous Atmospheric Chemistry. *J. Phys. Chem. B* **2001**, *105*, 10468−10472.
(96) Hofmeister, F. About Regularities in the Protein Precipitating Effects of Salts and the Relation of These Effects with the Physiological Behaviour of Salts. *Arch. Exp. Pathol. Pharmakol.* **1887**, *24*, 247−260.
(97) Sung, J. H.; Park, K.; Kim, D. Surfaces of Alcohol−Water Mixtures Studied by Sum-Frequency Generation Vibrational Spectroscopy. *J. Phys. Chem. B* **2005**, *109*, 18507−18514.
(98) Allen, H. C.; Casillas-Ituarte, N. N.; Sierra-Hernandez, M. R.; Chen, X.; Tang, C. Y. Shedding Light on Water Structure at Air−Aqueous Interfaces: Ions, Lipids, and Hydration. *Phys. Chem. Chem. Phys.* **2009**, *11*, 5538−5549.
(99) Baldelli, S.; Schnitzer, C.; Shultz, M. J. The Structure of Water on HCl Solutions Studied with Sum Frequency Generation. *Chem. Phys. Lett.* **1999**, *302*, 157−163.
(100) Bian, H.-t.; Feng, R.-r.; Xu, Y.-y.; Guo, Y.; Wang, H.-f. Increased Interfacial Thickness of the NaF, NaCl and NaBr Salt Aqueous Solutions Probed with Non-Resonant Surface Second Harmonic Generation (SHG). *Phys. Chem. Chem. Phys.* **2008**, *10*, 4920−4931.
(101) Chen, X.; Yang, T.; Kataoka, S.; Cremer, P. S. Specific Ion Effects on Interfacial Water Structure near Macromolecules. *J. Am. Chem. Soc.* **2007**, *129*, 12272−12279.
(102) Clarke, R. J.; Lupfert, C. Influence of Anions and Cations on the Dipole Potential of Phosphatidylcholine Vesicles: A Basis for the Hofmeister Effect. *Biophys. J.* **1999**, *76*, 2614−2624.
(103) Jungwirth, P.; Winter, B. Ions at Aqueous Interfaces: From Water Surface to Hydrated Proteins. *Annu. Rev. Phys. Chem.* **2008**, *59*, 343−366.
(104) Kalra, A.; Tugcu, N.; Cramer, S. M.; Garde, S. Salting-In and Salting-Out of Hydrophobic Solutes in Aqueous Salt Solutions. *J. Phys. Chem. B* **2001**, *105*, 6380−6386.
(105) Petersen, P. B.; Saykally, R. J. On the Nature of Ions at the Liquid Water Surface. *Annu. Rev. Phys. Chem.* **2006**, *57*, 333−364.
(106) Tian, C.; Ji, N.; Waychunas, G. A.; Shen, Y. R. Interfacial Structures of Acidic and Basic Aqueous Solutions. *J. Am. Chem. Soc.* **2008**, *130*, 13033−13039.
(107) Zhang, Y.; Cremer, P. S. Interactions Between Macromolecules and Ions: The Hofmeister Series. *Curr. Opin. Chem. Biol.* **2006**, *10*, 658−663.
(108) Aveyard, R.; Saleem, S. M. Salt Effects on Adsorbed Non-Electrolytes. *Can. J. Chem.* **1977**, *55*, 4018−4027.
(109) Bostrom, M.; Williams, D. R. M.; Ninham, B. W. Specific Ion Effects: Why DLVO Theory Fails for Biology and Colloid Systems. *Phys. Rev. Lett.* **2001**, *87*, 168103.
(110) Bostrom, M.; Williams, D. R. M.; Ninham, B. W. Special Ion Effects: Why the Properties of Lysozyme in Salt Solutions Follow a Hofmeister Series. *Biophys. J.* **2003**, *85*, 686−694.